J Mater Sci (2009) 44:114–121
DOI 10.1007/s10853-008-3098-8

Effect of shielding gases on mechanical and metallurgical properties of duplex stainless-steel welds

P. Sathiya · S. Aravindan · R. Soundararajan · A. Noorul Haq

Received: 7 August 2008 / Accepted: 30 October 2008 / Published online: 5 December 2008

Abstract Duplex stainless steels (DSS) are well known for their higher mechanical strength and better corrosion resistance. DSS is commonly used in the marine construction, petrochemical, and chemical industries. DSS (2205) has equal amounts of α and γ phases. However, unlike the parent metal, the solidification microstructure of the fusion zone in the weld does not have nearly equal amounts of the α and γ phases. Thus the mechanical properties and corrosion resistance of DSS welds are degraded. The interpass temperature plays a vital role in achieving balanced α and γ phases, which in turn results in improved mechanical and corrosion resistance. Gas tungsten arc welding (GTAW) is employed for welding of thin sheets/plates. The GTAW process ensures small amounts of slag formation during welding, which eliminates slag crevices and sites for corrosion attack. Standard 2205 (UNS S31803) DSS sheets of 5 mm thickness, with 22.37% Cr and 5.74% Ni, were used in this study. Weld beads were produced with Zeron-100 super DSS filler wire with higher alloy content (26% Cr and 8% Ni). Argon (Ar) and helium (He) were employed as shielding gases. Heat input was maintained <1 kJ/mm. Interpass temperatures were maintained at 120°C. The ferrite number of the weld metal for the two different shielding gases was investigated. Mechanical properties of joints such as impact strength and hardness were evaluated. Microstructure evaluation was also carried out.

P. Sathiya (✉) · R. Soundararajan · A. Noorul Haq
Department of Production Engineering, National Institute of Technology, Tiruchirappalli 620015, Tamil Nadu, India
e-mail: psathiya@nitt.edu

S. Aravindan
Department of Mechanical Engineering, Indian Institute of Technology Delhi, New Delhi 110016, India

Introduction

Tungsten inert-gas (TIG) welding uses a nonconsumable tungsten electrode and an inert gas for arc shielding. It is commonly used for fabricating joints of difficult-to-weld metals such as aluminum and stainless steels. Since the weld pool geometry plays an important role in determining the mechanical properties of the weld, this aspect strongly influences TIG weld quality [1]. A nonconsumable tungsten electrode, shielded by an inert gas, is used to strike an electric arc with the base metal (BM), providing the heat necessary to melt the BM. The quality of TIG weld is higher than that of any of the arc welding processes due to the reliability and strength of the welded joints. The gas tungsten arc welding (GTAW) process ensures small amount of slag formation during welding, which eliminates slag crevices and sites for corrosion attack [2]. Duplex stainless steels (DSS) consist of nearly equal amounts of ferrite and austenite phase at room temperature. DSS exhibits greater toughness and better weldability than ferritic stainless steel. DSS 2205 provides pitting and crevice corrosion resistance superior to that of 316L or 317L austenitic stainless steels in almost all corrosive media. The yield strength of DSS is about twice that of austenitic stainless steel. This allows a designer to save weight and makes the alloy more cost competitive when compared with 316L or 317L austenitic stainless steels. DSS is mainly used in the marine industry, in cargo tanks for ships and trucks, for power generation applications, and in pressure vessels, tanks piping, and heat exchangers in the chemical processing industry. Though the cost of processing of DSS is lower than that of austenitic stainless steel, maintaining equal amounts of ferrite and austenite phases is crucial. The Schaeffler diagram and WRC-1992 can be used for prediction of the ferrite content in the weld

metal. The Schaeffler diagram, now 50 years old, is out of date for ferrite prediction in stainless-steel welds. Since 1995, the WRC-1992 diagram has been recommended for ferrite prediction. This diagram is based on the nickel and chromium equivalent to asses the effects of addition of alloying elements on microstructural constituents of stainless-steel weld metal [3].

The main advantages of DSS are the equal amounts of α and γ phases present in the steel. Unlike the parent metal, the weld metal microstructure dose not have equal amounts of α and γ phases. For this reason, the mechanical properties and corrosion resistance of the DSS weld is degraded. This can be attributed to the reduction of the γ phase in the fusion zone. Interpass temperature is very important to achieve a structure with balanced α and γ phases. The ferrite-to-austenite ratio also depends on the heat input of the welding process. It has been reported that the problem of low fraction of γ phase in the weld metal can be alleviated by addition of nitrogen gas with different combinations in the plasma and laser beam, or by alloy addition in filler materials and even by carrying out post-weld heat treatment in the α/γ coexistence temperature range of 800–1,150°C [4].

Faster cooling rate significantly affects the fusion zone microstructure in pulsed GTAW welding for the same heat input condition [5]. Nickel is very effective in controlling the ferrite-to-austenite ratio compared with the cooling rate for the range of compositions studied [6]. Ferrite contents greater than 90% have been reported in electron beam welding (EB) in UNS 31803 [7]. It is thus desirable to control welding conditions such that cooling should be slow enough for adequate austenite formation, but fast enough to prevent deleterious precipitation. An acceptable phase balance may still be achieved, however, by the use of preplaced nickel foils [8] or through post-weld solution treatment, as recommended for laser welded super DSS [9]. Interpass temperature should be maintained at a specific value in order to alleviate the faster cooling rate over the temperature range 300–500°C, which is the critical region for phase transformation to occur in selective identification feature (SIF) 2205 DSS [10, 11]. This paper describes the effect of two different shielding gases (argon and helium) on mechanical and metallurgical characteristics of the welded joint.

Experimental details

The size of the base material chosen for this investigation was $90 \times 45 \times 5$ mm^3 sheets corresponding to UNS S31803, with chemical composition as given in Table 1. Zeron-100 filler wire with a diameter of 3 mm was used in this study; its chemical composition is also presented in Table 1.

Welding was performed with two different shielding gases (argon and helium) with two different welding parameters. The welding parameters were chosen in such a way as to keep the heat input below 1 kJ/mm. The details of the welding parameters are presented in Table 2.

The interpass temperature was maintained as 120°C. The ferrite content of the weld metal was estimated by the point count method. The ferrite percentages were determined metallographically using the point count method by following ASTM E 562 standards. Metallographic examinations were carried out by using optical microscopy. For metallographical examination, the samples were polished and electrolytically etched in 40% KOH solution. This etching was performed at 2 V for 15 s. In all cases, the austenite phase is seen as white while the dark phase is ferrite. The microhardness of weldment was measured from the BM, across the heat-affected zone (HAZ) to the weld zone (WZ), in transverse direction using a Metco SMV 1000 micro Vickers hardness machine under 1-kg load, maintained for 15 s. Charpy impact tests were performed to asses the notch toughness of samples extracted from the weldment. Notches were made such that fracture occurred only with in the weld fusion zone. The impact tests were performed both at room temperature and at -40°C on subsized samples ($55 \times 10 \times 4$ mm^3). The fractured surfaces of impact tested surfaces were studied using scanning electron microscopy (SEM) fractography.

Table 2 Welding parameters

	Argon	Helium
Current intensity (A)	135	140
Voltage (V)	11	12
Weld speed (mm/min)	100	110
Heat input (kJ/mm)	0.891	0.916
Gas flow rate (lpm)	10	10

Table 1 BM, filler wire (FW), and weld metal chemical composition (wt%)

Element (%)	C	S	P	Si	Mn	Cr	Ni	Mo	N	Fe
Base material	0.020	0.025	0.021	0.4	1.52	22.37	5.74	2.85	0.171	Balance
Filler wire	0.013	0.001	0.017	0.51	1.51	26.0	8.0	3.14	0.15	Balance
Weld metal—Ar	0.018	0.020	0.020	0.44	1.50	22.82	7.84	3.01	0.146	Balance
Weld metal—He	0.020	0.022	0.019	0.48	1.54	22.60	8.02	2.95	0.158	Balance

Results and discussion

The microstructure of as-received 2205 DSS as observed optically consists of elongated α and γ grains, as shown in Fig. 1; the morphology of the α–γ grain boundary is relatively smooth. The elongated α and γ phases have a grain size of about 45–50 μm in length and about 15 μm in width. The measured volume fractions of α and γ phases are almost equal.

A macrograph of the welded samples, with argon and helium shielding, is presented in Fig. 2. The helium-shielded weld bead has a wider width compared with that using argon.

In order to improve understanding, weld bead profiles were measured by using a "cam scope" and the profiles are presented in the Fig. 3a and b. From Fig. 3a it can be observed that the bead width of the argon-shielded weld is 12.43 mm and the depth of penetration is 4.499 mm. From Fig. 3b it can be observed that the bead width of the helium-shielded weld is 18.82 mm and the depth of penetration is 4.556 mm. The greater penetration and wider bead width achieved by using helium shielding is due to the higher arc energy. Compared with argon, helium provides better side-wall penetration and greater welding speeds by generating an energy-rich arc.

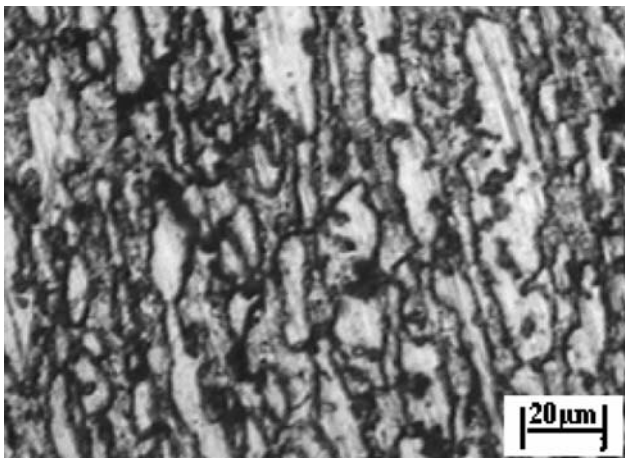

Fig. 1 BM microstructure

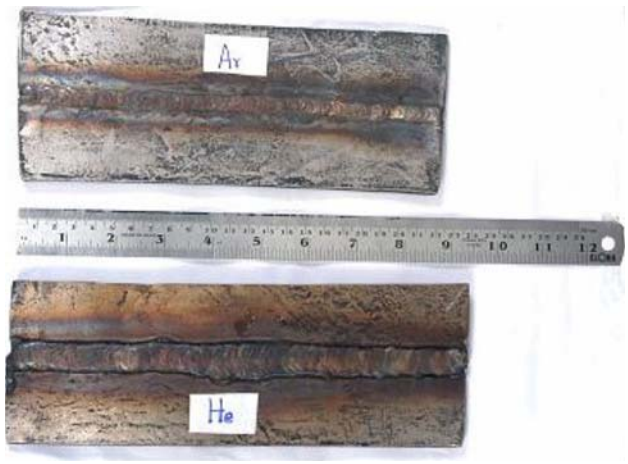

Fig. 2 Macrograph of the weld joint

Effects of chemical composition on DSS weld metal

The ferrite-to-austenite ratio in DSS weld metal is determined by the chemical composition and the cooling rate experienced during welding. Cooling rate is a function of weld geometry. Heat input and preheat temperature depend on the type of welding and the process parameters employed. Filler wire chemical composition, the nature of the shielding gas, and the degree of dilution determine the composition of the weld metal. Two different shielding gases were used and the corresponding weld metal chemical compositions are presented in Table 1.

From Table 1 it can be seen that the fraction of ferrite-stabilizing elements such as Cr and Mo is greater in the argon-shielded weld whereas the fraction of the austenitic-stabilizing elements Ni and N is greater in the helium-shielded weld metal. All DSS weld metals solidify primarily as ferrite and, in the subsequent solid-state transformation, part of the ferrite transforms to austenite. This ferrite-to-austenite transformation takes place over a range of temperatures. However, the transformation cannot attain equilibrium due to rapid cooling, so that more ferrite remains untransformed than under equilibrium conditions. The transformation of ferrite to austenite during the welding of DSS is similar to that in low-carbon-steel weld metals in which austenite transforms to ferrite on cooling. However, a major difference exists between the transformations in low-carbon steels and DSS. In low-carbon steels all of the austenite is transformed to a combination of ferrite, bainite, and martensite, except for a small amount of retained austenite when present. However, in DSS, a considerable volume of ferrite remains untransformed. The solidification models of the two investigated shielding gas weld metals were calculated from their corresponding chromium and nickel equivalents. The solidification mode for both of the shielding gases was ferrite.

The Cr and Ni equivalents were calculated by using the following formulae (with values presented):

$$\begin{aligned} \mathrm{Cr_{eq}} &= \%\mathrm{Cr} + \%\mathrm{Mo} + 0.7\%\,\mathrm{Nb} \\ &\quad (\text{Argon - } 25.83\,\&\,\text{Helium - } 25.55, \\ &\quad \mathrm{Cr_{eq}}/\mathrm{Ni_{eq}} = 2.26), \\ \mathrm{Ni_{eq}} &= \%\mathrm{Ni} + 35\%\,\mathrm{C} + 20\%\,\mathrm{N} + 0.25\%\,\mathrm{Cu} \\ &\quad (\text{Argon - } 11.39\,\&\,\text{Helium - } 11.88, \\ &\quad \mathrm{Cr_{eq}}/\mathrm{Ni_{eq}} = 2.15). \end{aligned}$$

From these values, it can be clearly seen that the chromium and nickel equivalents are higher in the

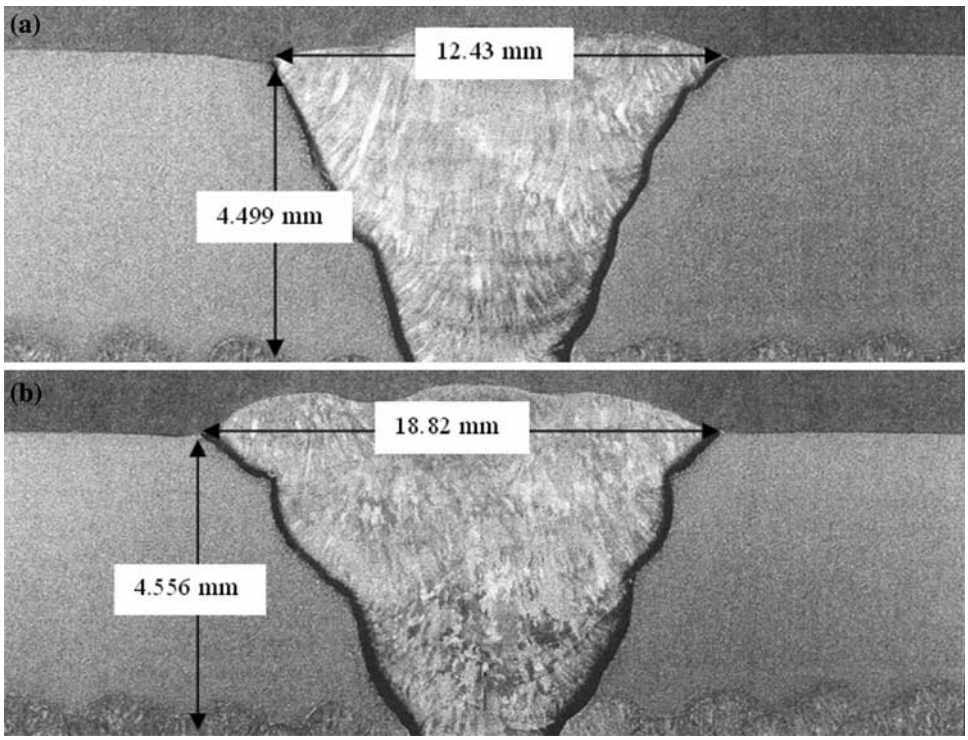

Fig. 3 Weld bead profile: **a** argon shielding gas and **b** helium shielding gas

argon-shielded weld metal. Due to the high Cr_{eq}/Ni_{eq} ratios, a large amount of ferrite is present in the argon-shielded weld. This is further confirmed by superimposing the Cr_{eq}/Ni_{eq} ratios of the weld metals on a pseudobinary diagram, which confirms that the mode of solidification is ferrite. The WRC-1992 (Fig. 4) diagram is used for estimating weld-metal ferrite on the basis of chemical composition. The ferrite content based on the ferritoscopic analysis for both of the shielding gases is indicated in Fig. 4. In the same diagram the ferrite content calculated from the Cr_{eq} and Ni_{eq} values is also presented.

Charpy V-notch impact test

The Charpy impact toughness of the DSS parent material is 85 J. The TIG welded specimens were tested at room and subzero temperature (−40°C). The toughness of the test results welded with different shielding gases is tabulated in Table 3.

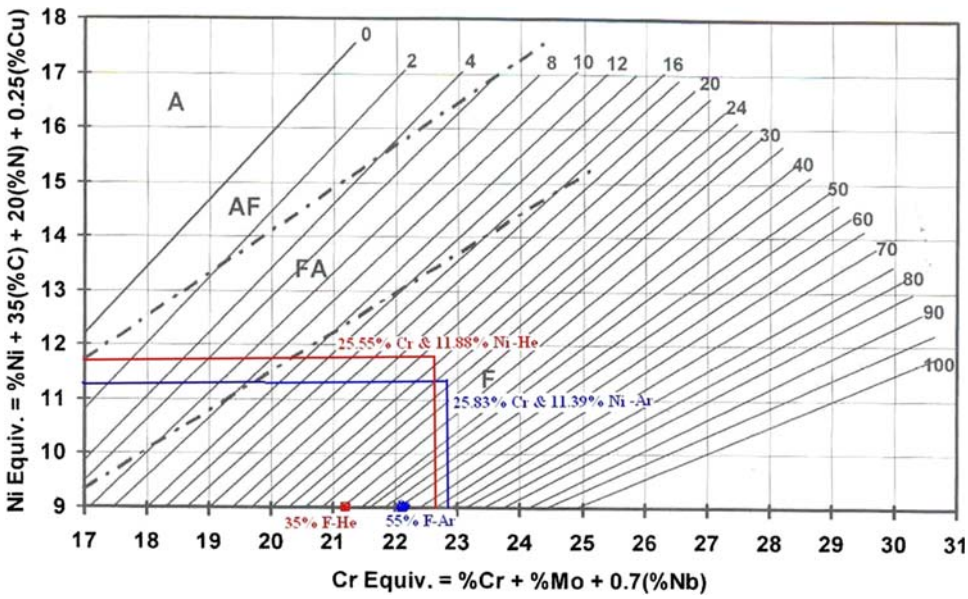

Fig. 4 WRC-1992 diagram [12]

Table 3 Impact test results

Temperature (°C)	Impact values (J)	
	Argon gas	Helium gas
25	87	92
−40	65	78

Three samples were tested at room temperature and at −40°C, and the average values are tabulated in Table 3. The helium-shielded weld sample exhibited higher toughness than did the argon-shielded weld. The reasons for this can be attributed to the cooling rate, the larger amount of arc energy, and the presence of larger amounts of Mn in the WZ. In general, increase of the ferrite content of the weld metal decreases its toughness. Argon-shielded welds have a larger amount of ferrite phase whereas helium-shielded welds have a greater amount of austenite-stabilizing elements such as Ni and N. Hence, the helium-shielded weld has a greater amount of austenite phase and exhibits higher toughness than the argon-shielded weld. Manganese is one of the powerful alloying elements for improving the toughness of the weld metal. The observed differences in toughness were not only due to changes in the ferrite content, but also due to the reduction in the ferrite-to-austenite ratio. The decrease in toughness values at the subzero temperature for both of the weld metals can be attributed to the presence of ferrite, which suffers from a ductile brittle transition [13]. The impact toughness of the DSS weldment deteriorates with increasing volume of α-ferrite within the HAZ [14]. Careful control of heat input and interpass temperatures during welding are required to correct the α-to-γ ratio in the DSS weld. Less heat input results in a faster cooling rate, preventing the transformation of primary α into γ phase in the weld [15]. The low γ content in the fusion zone is responsible for its poor impact toughness [16]. The results of impact SEM fractography are presented in Fig. 5a–d. For all of the impact fractured specimens, the grains are elongated in the grain-boundary direction and fine dimples are present on the fractured surfaces, revealing that the ductile fracture mode with fine dimples occurred in the fracture of welds with both shielding gases.

Hardness testing

The samples were prepared and electrolytically etched with 40% KOH solution. Three distinguished zones were identified and a set of ten microhardness readings was taken in each. The average values are presented in Table 4.

From Table 4 it can be clearly seen that the hardness of the weld metal is slightly higher than that of the HAZ and the base material for both the argon- and helium-shielded cases. The hardness of the argon-shielded weld is less than that of the helium-shielded weld, since the Ar-shielded welds have less austenite phase compared with the helium-shielded weld metal. It has been reported that the ferrite and austenite phases do not differ greatly in composition

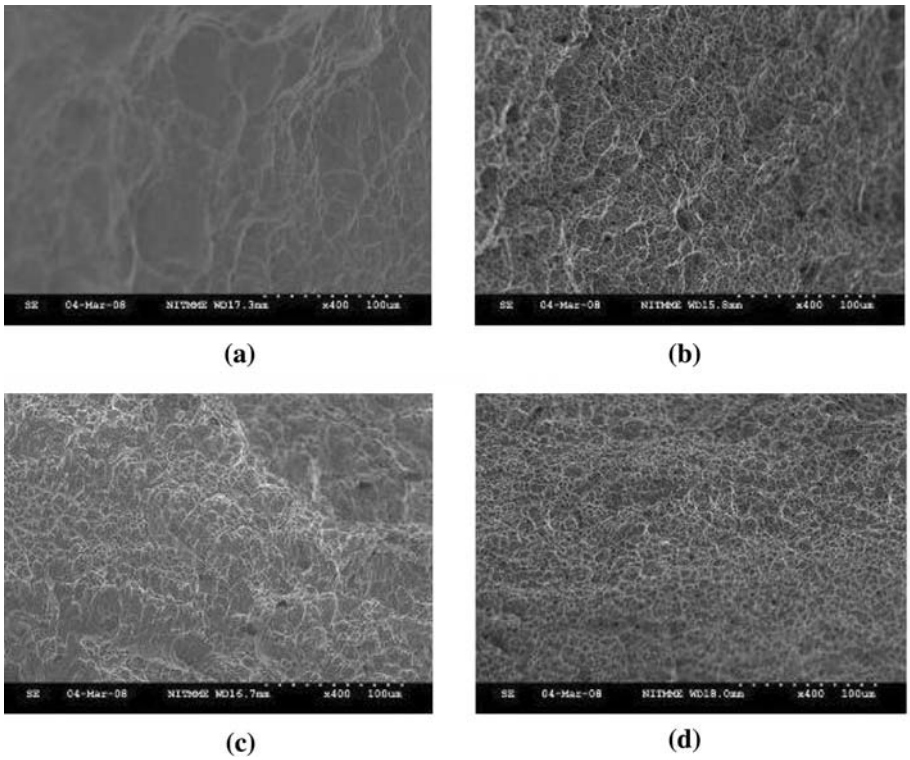

Fig. 5 SEM fracture surface of impact tested specimens. **a** −40°C with argon shielding gas. **b** Room temperature with argon shielding gas. **c** −40°C with helium shielding gas. **d** Room temperature with helium shielding gas

Table 4 Average microhardness values

Serial no.	Shielding gas	Microhardness value (VHN)		
		BM	HAZ	Weld metal
1	Argon	173	259	308
2	Helium	174	283	325

because substitutional elements do not have time to partition significantly during DSS welding.

The authors have conducted investigations on several commercial and experimental alloys to understand the effect of nitrogen on strengthening of DSS and concluded that, if the fraction of nitrogen in DSS is <0.13%, ferrite is harder than austenite, whereas for a nitrogen content of 0.13% in DSS, the hardness levels of austenite and ferrite are equal and austenite becomes harder than ferrite when the nitrogen content exceeds 0.13% [17]. In the present study the nitrogen content of the weld metals for both the argon- and helium-shielded weld metals exceeded 0.13%. Therefore, in these weld metals austenite is harder than ferrite.

Ferrite measurement

There are two methods for measuring the ferrite content of weld metals: the point count procedure and a magnetic method using a Fisher ferrite scope. The advantage of the point counting method is that it can be applied to all microstructures, including the narrow HAZ. However, it is difficult to apply in situ and is relatively expensive. In this work Fisher ferrite scope was used. In the case of the argon-shielded GTA weld, the ferrite content is estimated to be 55% while the remaining 45% in the weld metal is austenite. Due to nitrogen loss as well as the lower amount of austenite-stabilizing elements, as seen in Table 3, the amount of austenite phase is lower in the argon-shielded weld metal. In the helium-shielded weld metal the amount of austenite-stabilizing elements was higher than in the argon-shielded weld metal. A similar effect is also observed in the microstructure; as shown in Fig. 7c and d the austenite phases comprised 65% of the helium-shielded weld metal and while the remaining 35% was ferrite phase.

Microstructural studies

The microstructure of the welds with different shielding gas is presented in Fig. 6a–d.

When using pure argon as the shielding gas in GTAW joints, the result is normally nitrogen loss and a high amount of ferrite-stabilizing element present. Due to this the balance between the two phases is not even. As shown in Fig. 6a, a large amount of ferrite phase is present in the microstructure. As an effective stabilizer of austenite,

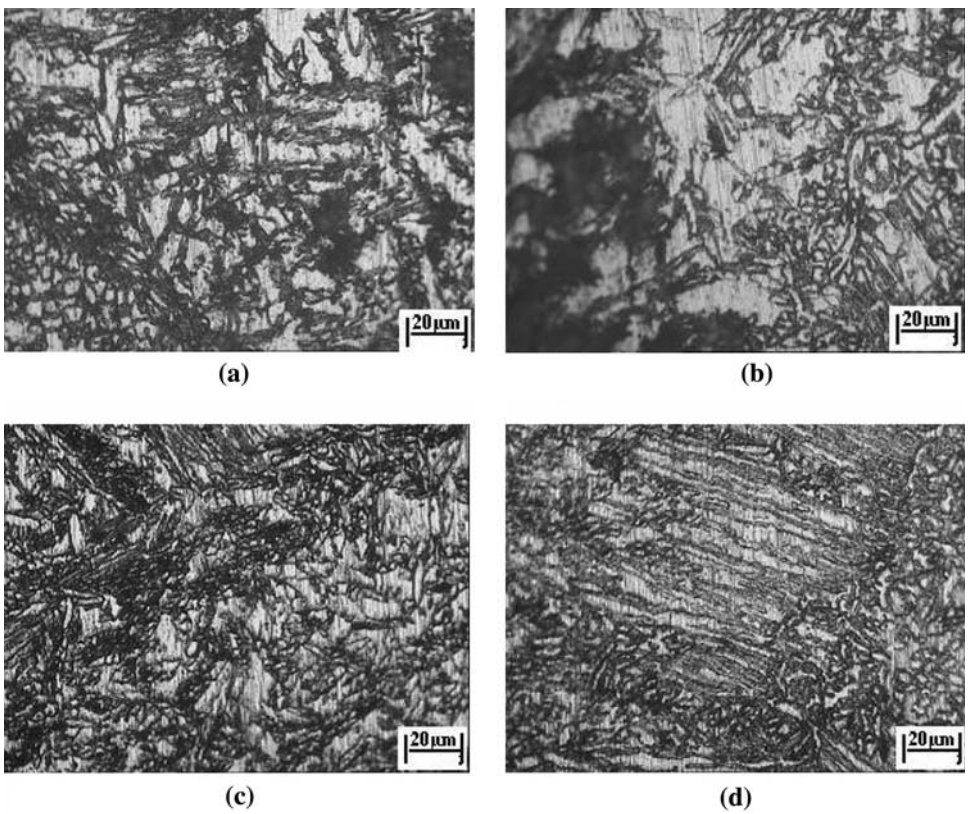

Fig. 6 Weld metal and HAZ microstructures. **a** Argon shield, weld metal (200×). **b** Argon shield, HAZ (200×). **c** Helium shield, weld metal (200×). **d** Helium shield, HAZ (200×)

nitrogen has played an important role in the development of DSS. Many studies on high-nitrogen grades have been reported, especially in terms of improvement of mechanical and corrosion properties [18–21]. The weldability of DSS has been improved by the addition of nitrogen to stabilize austenite at elevated temperature [22]. In general, the austenite phase in DSS weld metal is formed from ferrite in three modes: allotrimorphs at the prior-ferrite grain boundaries, Widmanstätten side-plates growing into the grains from these allotrimorphs, and intragranular precipitates. The possibility of chromium nitride formation during welding of DSS has been reported [23]. In the described study pure argon and helium were used as the shielding gas. From the previous literature said pure argon as shielding gas, which is occurred in the nitrogen loss. Hence, it can be avoid for the nitrogen loss we can properly maintained by the heat input and interpass temperature, can control the nitrogen loss in the weld metal. By appropriate selection of the heat input and interpass temperature, one can achieve a less significant difference in the amount of α and γ phases (55% ferrite and 45% austenite) present in the Ar-shielded weld metal compared with the helium-shielded weld. Chromium nitride precipitations can also be observed in Fig. 7.

More ferrite phase was present in argon-shielded weld metal. So, the solubility of nitrogen in ferrite decreases rapidly with decreasing temperature. A significant amount of the ferrite phase is observed, and also it can be clearly seen that the grains in the argon-shielded weld metal are finer (Fig. 6a). The austenitic phases seen within the grains could be either intragranular precipitates or Widmanstätten austenite transverse to the long-axis direction, as shown in Fig. 6d. Widmanstätten austenite also nucleates directly from prior α-ferrite boundaries which have not been covered by allotrimorphic austenite perturbation. Widmanstätten austenite has a much higher aspect ratio (length/thickness). The large amount of austenite phase present is due to the high Mn content and the large amount of austenite-stabilizing elements present in the weld metal (Fig. 6c, d). Due to the energy-rich arc, a greater amount of Widmanstätten austenite structure was presented in the helium-shielded WZ compared with in the Ar-shielded WZ.

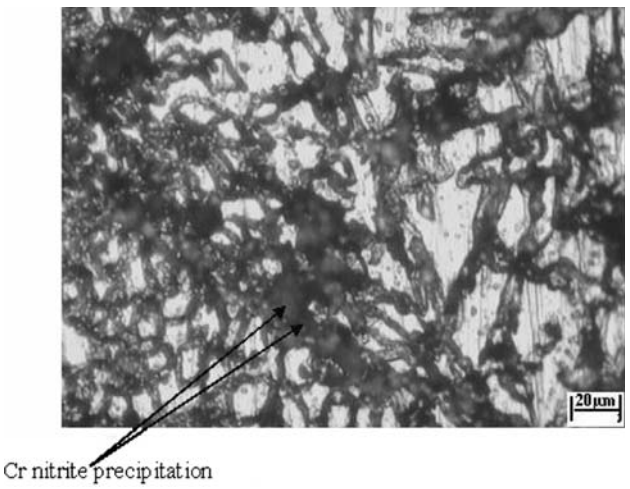

Fig. 7 Argon-shielded weld with chromium nitride precipitations (200×)

Conclusions

DSS weld metals with different shielding gases were welded and examined, the results are as follows:

(1) When using the helium shielding gas the weld bead aspect ratio (width/penetration) is higher than in the Ar-shielded weld.
(2) Helium-shielded welds exhibited higher toughness due to the large Mn content and the smaller amount of ferrite phase and larger amount of austenite phase present in the weld metal.
(3) Due to the high value of the Cr_{eq}/Ni_{eq} ratio, a large amount of ferrite is present in the argon-shielded weld metal.
(4) Chromium nitride precipitation is observed in the argon-shielded weld metal.
(5) For the argon-shielded weld metal an even phase balance (55% ferrite and 45% austenite) can be achieved by appropriate selection of the heat input and interpass temperature.
(6) The hardness of the weld metal is much higher than that of the BM and HAZ for both studied shielding gases.
(7) Due to the high arc energy the Widmanstätten austenite structure was present in the microstructure of the helium-shielded weld.

Acknowledgement The authors would like to express their heartfelt thanks to Mr. P. Veerappan, Proprietor, Keerthana Engineering Works, Tiruchirappalli-15, Tamil Nadu, India, for conducting the welding trials in his factory.

References

1. Folkhard E (1988) Welding metallurgy of stainless steel. Springer-Verlag, Vienna, p 186
2. Karlsson L, Ryen L, Pak S (1995) Weld J 74(11):28s
3. Kotecki DJ (2000) Weld J 79(12):346s
4. Hilkes J, Bekkers K (1995) Weld J 74(11):51
5. Badij R, Belkessa B, Maza H, Bouabdallah M, Bacroix B, Kahloun C (2004) Mater Sci Forum 217:467
6. Wang S-H, Chiu P-K, Yang J-R, Fang J (2006) Mater Sci Eng A 420:26
7. Muthupandi V, Bala Srinivasan P, Seshadri SK, Sundaresan S (2003) Mater Sci Eng A 358:9

8. Bonnefois B, Charles J, Dupoiron F, Soulignac A (1991) Proceedings of the conference on duplex stainless steels '91, vol 1, Beaune, France, p 347
9. Bonollo F, Tiziani A, Zambon A, Penasa M (1994) Proceedings of fourth international conference on duplex stainless steels, paper 108, vol 2, Glasgow, Scotland, p 13
10. Brown EL, Burnett ME, Purtscher PT, Krauss G (1983) Metall Mater Trans A 14:791
11. Zambon A, Bonollo F (1994) Mater Sci Eng A 178:203
12. Kou S (2003) Welding metallurgy, 2nd edn. Wiley, Hoboken, NJ, p 225
13. Ramirez AJ, Lippold JC, Brandi SD (2003) Metall Mater Trans A 34:1575
14. Gooch TG (1982) ASM conference on duplex ferritic-austenitic stainless steels, St. Louis, p 573
15. Ku JS, Ho NJ, Tjong SC (1997) J Mater Process Technol 63:770
16. Honeycombe J, Gooch TG (1978) Proceedings of trends in steels and consumables, The Welding Institute, London, p 28
17. Wahlberg G, Dunlop GL (1987) Proceedings of the conference on stainless steels, The Institute of Metals, University of New York, p 291
18. Hertzman S, Jargelius Pettersson R, Blom R, Kivineve E, Eriksson J (1996) ISIJ Int 7(36):968
19. Siegmund T, Werner E, Fisher FD (1993) Comput Mater Sci 1:234
20. Kokawa H, Tomita M, Kuwana T (1995) Weld Int 9(3):8
21. Ogawa T, Koseki T (1989) Weld J 68:181s
22. Charles J (1991) Proceedings of the conference on duplex stainless steels '91, Les editions de physique, Beaune, p 3
23. Ogawa K, Komizo Y, Azuma S, Kudo T (1992) Trans Jpn Weld Soc 23(1):40